LIMNOLOGY
and
OCEANOGRAPHY

ASLO

Limnol. Oceanogr. 9999, 2025, 1–15

doi: 10.1002/lno.70001

RESEARCH ARTICLE

Daily Sun-induced chlorophyll fluorescence vs. irradiance curves reflect the photoadaptation of phytoplankton in surface waters

Yannick Huot [1*], **David Antoine** [2,3], **Vincenzo Vellucci** [4,5]

[1]Département de géomatique appliquée, Université de Sherbrooke, Québec, Canada; [2]Remote Sensing and Satellite Research Group, School of Earth and Planetary Sciences, Faculty of Science and Engineering, Curtin University, Perth, Western Australia, Australia; [3]Sorbonne Université, CNRS, Laboratoire d'céanographie de Villefranche, LOV, Villefranche-sur-Mer, France; [4]Sorbonne Université, CNRS, Institut de la Mer de Villefranche, IMEV, Villefranche-sur-Mer, France; [5]Sorbonne Université, CNRS, OSU Station Marines, STAMAR, Paris, France

Abstract

Phytoplankton chlorophyll Sun-induced fluorescence is observable in the upwelling light field of the ocean. This allows its observation by radiometers in situ or on satellite sensors. Since it is influenced by both biomass and physiology it can potentially provide information about both. Since fluorescence yield is complementary to photosynthesis and heat in photosystem II, its observation throughout the day provides information on the response of phytoplankton to diel light cycles. Here we use a time series collected in the northwestern Mediterranean Sea (BOUSSOLE site) to extract photophysiological parameters of phytoplankton using the Sun-induced fluorescence and as well as with an active chlorophyll fluorometer. The daily resolved patterns are consistent with photoacclimation and photoadaptation processes and reflect seasonal variations of the mixed-layer average irradiance. We also show that fluorescence yields derived from satellite measurements (MODIS) at the same location are not correlated to these patterns, confirming the limited influence of photoacclimation and photoadaptation on the satellite-derived chlorophyll fluorescence yield near solar noon.

The Sun-induced fluorescence has long been proposed as an in situ or remotely observable variable that could provide insights into the photophysiology of phytoplankton and provide direct or indirect information on primary production efficiency (Kiefer, Chamberlin, and Booth 1989; Chamberlin et al. 1990; Chamberlin and Marra 1992). These studies formed part of the basis for launching ocean color satellites (MODIS, MERIS, and successors) with spectral bands dedicated to the measurement of Sun-induced fluorescence (Abbott and Letelier 1999). Despite years of research, the unconstrained relationship between the quantum yield of photosynthesis and the apparent quantum yield of fluorescence has shown that such an approach is impractical (Falkowski and Kolber 1995). This is especially true when using Sun-synchronous satellites that take measurements near noon, which then reflect complex non-photochemical processes (Lin et al. 2016). This does not mean that the Sun-induced fluorescence measurements are not useful. Their specificity to phytoplankton makes them a unique remote sensing measurement of a signal originating unequivocally from phytoplankton. It has been also proposed and used as a proxy of nutrient limitation (Letelier, Abbott, and Karl 1997; Behrenfeld et al. 2009; Browning, Bouman, and Moore 2014; Browning et al. 2023; Schallenberg et al. 2020).

Until the launch of the Korean Geostationary Ocean Color Imager (GOCI) sensor in 2010 (and GOCI-II in 2020), all ocean color satellite sensors were placed on Sun-synchronous orbits (Ryu et al. 2012) and provided approximately one measurement per day usually near solar noon. These geostationary ocean color sensors deliver multiple measurements of the same area several times throughout the day and allows,

*Correspondence: yannick.huot@usherbrooke.ca

Associate editor: Ilana Berman-Frank

Data Availability Statement: The in situ data used in this paper is available at http://www.obs-vlfr.fr/Boussole/html/boussole_data/login_form.php and are in the process of being prepared for an archival system. The satellite data is available from https://oceancolor.gsfc.nasa.gov. Matlab processing codes are available upon request to Yannick Huot.

among other things, the measurement of diel cycles that are driven by biological processes (Wu et al. 2022).

Diel observation of chlorophyll fluorescence provides information on the relationship between the incident irradiance and the quantum yield of fluorescence. In doing so, they should provide an observation of the photoacclimation state of phytoplankton in the surface layer (O'Malley and Behrenfeld 2014). In this paper, we use the time series obtained from the BOUée pour l'acquiSition d'une Série Optique à Long termE (BOUSSOLE, Antoine et al. 2006) mooring to examine this hypothesis more closely and examine which, if any, variables can be extracted that are linked to the phytoplankton growth irradiance, and therefore their photophysiological state. We further examine how these photophysiological parameters are linked to the remotely sensed quantum yield.

Background

The reference state for fluorescence measurement is the maximum level of fluorescence of a system (*see* e.g., Huot and Babin 2010 for more details on concepts presented in this section). When fluorescence is below this level, it is referred to as quenched. Quenching occurs when an increasing fraction of the energy absorbed by pigments is used for processes that do not lead to fluorescence. In the case of in vivo chlorophyll fluorescence, this is by energy transfer to other molecules that either (1) dissipate the energy as heat (non-photochemical quenching, NPQ) or (2) use the energy for charge separation, the first step of photosynthesis (photochemical quenching).

Therefore, when phytoplankton absorb photons, the absorbed energy can follow three paths: photosynthesis (charge separation), heat or fluorescence. At low light, most of the energy absorbed is used for photosynthesis, some is dissipated as heat and a small fraction is released as chlorophyll fluorescence. This latter fraction is referred to as the (apparent) quantum yield of fluorescence (φ_f, photons emitted/photons absorbed), representing at most a few percent. This is the state with the most photochemical quenching. As irradiance further increases, the fraction going to photosynthesis decreases as the photosynthetic apparatus cannot use all the photons and more goes to heat and fluorescence; photochemical quenching decreases and φ_f increases. When the photosynthetic capacity of the phytoplankton becomes saturated by even higher irradiance, a suite of regulatory processes protects them from photodamage by allowing a greater dissipation of the absorbed energy as heat. This dissipation of the absorbed energy leads to a reduced fraction of the absorbed energy going to fluorescence and a decrease of φ_f; non-photochemical quenching of chlorophyll fluorescence increases. Figure 1a,b provides an illustration of these processes leading to a curve with a maximum at intermediate irradiance levels (increase of φ_f at low irradiance and decrease at high irradiance). Note that the absolute amount of Sun-induced fluorescence (e.g., measured as radiance) generally increases or reaches a plateau (*see* e.g., discussion in O'Malley and Behrenfeld 2014) with the amount of photons absorbed. It is only φ_f, the *fraction* of absorbed light going to fluorescence, that shows the patterns observed in Fig. 1a,b. To reflect changes in φ_f the fluorescence radiance is therefore divided by the downwelling irradiance at the depth of the sensor (which is proportional to the absorbed irradiance if the phytoplankton absorption coefficient does not change). Under these conditions, the measured fluorescence is equivalent to the steady-state light acclimated fluorescence parameters F' (or F_s) measured with variable fluorescence instruments such as fast repetition rate fluorometers (FRRF) and pulse amplitude modulation (PAM) fluorometers (Roháček 2002; Huot and Babin 2010). When measuring fluorescence with an active fluorometer, the irradiance to which phytoplankton are exposed is the sum of the ambient irradiance and that of the exciting light from the fluorometer.

Manufacturers use modulated or flashing light to isolate the fluorescence excited by sunlight such that the fluorescence observed is only from the constant excitation irradiance of the fluorometer. To increase the signal manufacturers generally use a bright light source that saturates the capacity of photosynthetic systems ("closes" photosystem II) to process photons and prevents the observation of photochemical quenching at low solar irradiance. This means that the increase in φ_f with increasing irradiance at low irradiance is not observed (*see* Fig. 1c). Due to water circulation near the fluorometer, phytoplankton are generally not exposed to the fluorometer exciting irradiance for a sufficiently long time to initiate non-photochemical processes (which require tens of seconds to minutes), the non-photochemical quenching from the solar irradiance is, however, present leading to a reduction of the fluorescence with increasing solar irradiance. At low ambient irradiance, these fluorometers will provide measurements that are similar to variable fluorometers (FRRF or PAM) F_m or F'_m, while at high irradiance it will depend on the excitation irradiance and will be somewhere between F' and F'_m (Huot and Babin 2010).

The φ_f vs. irradiance curve, like a photosynthesis vs. irradiance curve (Geider, MacIntyre, and Kana 1996; MacIntyre et al. 2002), responds to photoacclimation processes and nutritional status (Laney, Letelier, and Abbott 2005; Comeau 2010). The way in which the shape of the curves should change with acclimation, adaptation and community composition in the environment is, however, very hard to predict theoretically. For instance, different photoacclimation strategies can be adopted by the different species (Lutz et al. 2001; Simis et al. 2012) present under different irradiance, mixing, temperature and nutrient conditions (MacIntyre et al. 2002).

Methods

Data

BOUSSOLE mooring

The BOUSSOLE mooring was located at 7°54′E, 43°22′N in the Ligurian Sea (Northeast Mediterranean Sea). The buoy was designed to minimize its impact on radiometric measurements,

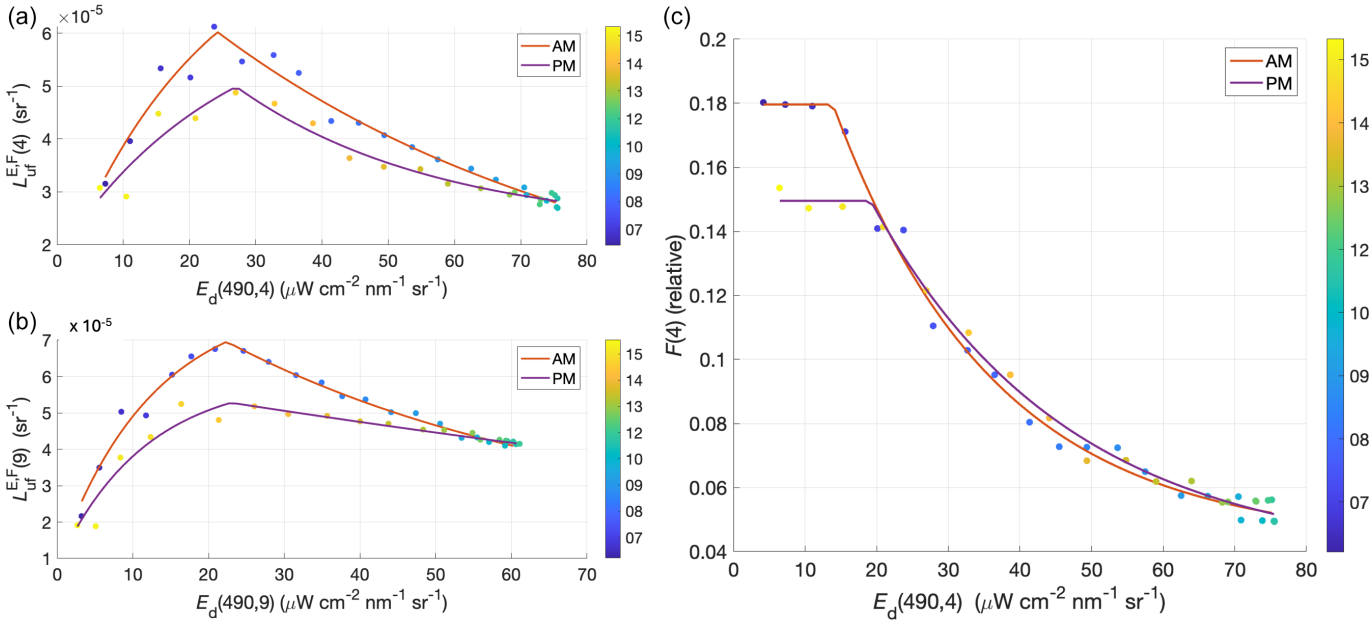

Fig. 1. Example of Sun-induced fluorescence at (**a**) 4 m and (**b**) 9 m measured with a multispectral radiometer (Satlantic OCR-200) and of (**c**) active fluorescence at 4 m from a standard chlorophyll fluorometer (WET Labs ECOFLNTUS) collected at the BOUSSOLE site on 23 October 2015. Color bar indicates the hour of the day. Though not measured directly, the changes in both measurements (*see* detail in text) during the day reflect mostly variations in the quantum yield of chlorophyll fluorescence.

that, combined with environmental conditions at the site, allow meeting requirements for the vicarious calibration of satellite measurements (Antoine et al. 2020). Here we describe only the parts used in this paper; for a full description of the system see Antoine et al. (2006). The upwelling radiance at nadir ($L_u(\lambda, z)$, μW cm^{-2} nm^{-1} sr^{-1}) and downward plane irradiance ($E_d(\lambda, z)$, μW cm^{-2} nm^{-1}) were measured underwater at 4 and 9 m depth (z) using multispectral radiometers (Sea-Bird scientific/Satlantic OCR-200 series). Active chlorophyll *a* fluorescence was measured using Sea-Bird scientific/WET Labs ECOFLNTUS fluorometers at 4 and 9 m with excitation at 470 nm and emission at 695 nm. Fluorometers were equipped with shutters to prevent biofouling. Two sets of radiometers containing each 7 wavelengths (λ) were used alternatively on two buoys that were swapped on site about every 6 to 12 months to allow calibration. The sets include 412.5, 442.5, 490, 510, 560, 670, 681 nm or 442.5, 490, 510, 555, 560, 665, 681 nm. The above-water downward plane irradiance was also measured for the same wavelengths. Data were collected every 15 min for 1 min for both radiometers (6 Hz) and fluorometers (1 Hz). The median value of the 1-min records is used for further analysis. Herein, we use the time series from the beginning of 2010 to the end of 2015. Hyperspectral radiometers (Sea-Bird scientific/Satlantic HyperOCR series) were also available on the mooring to measure the same variables at more wavelengths. Their integration time was, however, optimized for the blue and green bands where irradiance is much higher than in the red, and therefore provide noisy data in the red bands especially at low irradiance. A subset of these data (collected after 2016) will thus be used only to develop an approach to extract the fluorescence radiance ($L_{uf}(681, z)$, μW cm^{-2} nm^{-1} sr^{-1}) from the multispectral sensors. Copper tape was used to prevent biofouling on the radiometers. All instruments on the mooring were whether cleaned or swapped roughly every two weeks to further reduce biofouling. Post-processing was used to identify any data that may have suffered from biofouling by checking the data before and after the cleaning operation. Suspicious data was flagged and not used.

The band at 681 nm on the OCR-200 was designed to match the MERIS band at the same wavelength which was planned to study Sun-induced fluorescence. The standard procedure to extract Sun-induced fluorescence with multispectral data is to use a "baseline" approach (Neville and Gower 1977) whereby bands on either side of the fluorescence peak are used to define a baseline of "elastically scattered" photons and the height above this baseline is the measurement of fluorescence. However, the BOUSSOLE radiometers do not collect data beyond 681 nm. We used an alternative approach (*see* Schallenberg et al. 2008 for a related approach) using a multiple regression fit to estimate the radiance fluorescence at 681 nm using the measurement of $L_u(665, z)$ or $L_u(670, z)$ (depending on sensor set) and $L_u(681, z)$. Specifically, with the hyperspectral L_u collected at 4 and 9 m, we used the baseline approach to obtain $L_{uf}(681, z)$ and then regressed the $L_{uf}(681, z)$ as a function of $L_u(665, z)$ or $L_u(670, z)$ and $L_u(681, z)$ (i.e., $L_{uf}(681, z) = f(L_u(665, z)|L_u(670, z), L_u(681, z)) + \varepsilon$ where ε is the error term). We thus obtained two regressions, the first using $\lambda = 665$ and $\lambda = 681$ and the second using $\lambda = 670$ and $\lambda = 681$ that can be

used with the multispectral data to obtain $L_{uf}(681, z)$ using the two sets of instruments (*see* Fig. 2).

Once $L_{uf}(681, z)$ is obtained, we compute the irradiance-normalized fluorescence radiance (sr^{-1}): $L^{E}_{uf}(681,z) = L_{uf}(681,z)/E_d(490,z)$. Where $E_d(490,z)$, is the downwelling irradiance at the same depth as the $L_{uf}(681,z)$ measurements and provides an approximation of the fluorescence excitation irradiance. Furthermore, to reduce the impact of intraday changes in phytoplankton absorption (i.e., the phytoplankton abundance metrics that influences fluorescence) that could arise from growth, or changes in water masses on the parameter estimation (*see* below), we fit a linear regression on the active fluorescence measurement made between 00h00 and 3h00 the nights before and after each day when the $L^{E}_{uf}(681,z)$ are used (i.e., day time data are not used in this regression only the two night periods). We then normalize the data at each sampling time by the value of the regression computed at the time ($F_{reg}(t)$, unitless; the symbol "F" is used for the measurements from the fluorometer) and multiply it by the daily mean of the regression ($\overline{F}_{reg}$, unitless), $L^{E,F}_{uf}(681,z,t) = L^{E}_{uf}(681,z,t)\overline{F}_{reg}/F_{reg}(t)$. It is important to note that this does not normalize the emission for changes in phytoplankton absorption over the whole time series, but only for intraday variations. Therefore, while variability from the phytoplankton absorption is removed as much as possible over 1 d, to allow examining photophysiological changes, the amplitude of $L^{E,F}_{uf}(681,z,t)$ is still proportional to phytoplankton absorption between days. As such, it can be interpreted as a reflectance, where the normalization irradiance is at the excitation wavelength of fluorescence instead of at the same wavelength as the fluorescence emission.

MODIS data

Level 1a ocean color MODIS AQUA data were downloaded from NASA's Ocean color portal from the beginning of 2010 to the end of 2015. A 5 × 5 pixel region was extracted for the BOUSSOLE site location. From this dataset, chlorophyll *a* (D'Ortenzio et al. 2002; Hu, Lee, and Franz 2012), normalized fluorescence line height (Behrenfeld et al. 2009) and two estimates of the quantum yield of Sun-induced chlorophyll fluorescence (Behrenfeld et al. 2009; Huot, Franz, and Fradette 2013) were obtained. No correction for non-photochemical quenching is applied to either of the estimates. The normalized fluorescence line height (nflh, mW cm^{-2} μm^{-1} sr^{-1}) provides an estimate of fluorescence emission at the surface and is calculated as the difference between the measured nLw(678) and a linearly interpolated nLw(678) from two surrounding bands (~ 767 and ~ 750 nm). As such it is equal to $L_{wf}(681)F_0(681)/E_d(681,0^+)$, where $L_{wf}(681)$ is the fluorescence water leaving radiance and $F_0(681)$ is the spectral solar irradiance (constant) at the top of atmosphere (Thuillier et al. 1998). So while numerically different, the sources of variability in the signal are very similar to $L^{E}_{uf}(681)$ (and $L^{E,F}_{uf}(681)$). The Behrenfeld et al. (2009) algorithm is a semi-empirical approach that corrects for statistical trends in the optical characteristics of phytoplankton and water as a function of chlorophyll (blue to green reflectance ratio) while the Huot, Franz, and Fradette (2013) algorithm is a fully empirical algorithm. It accounts for the same statistical relationship and attempts to correct for biases caused by colored dissolved

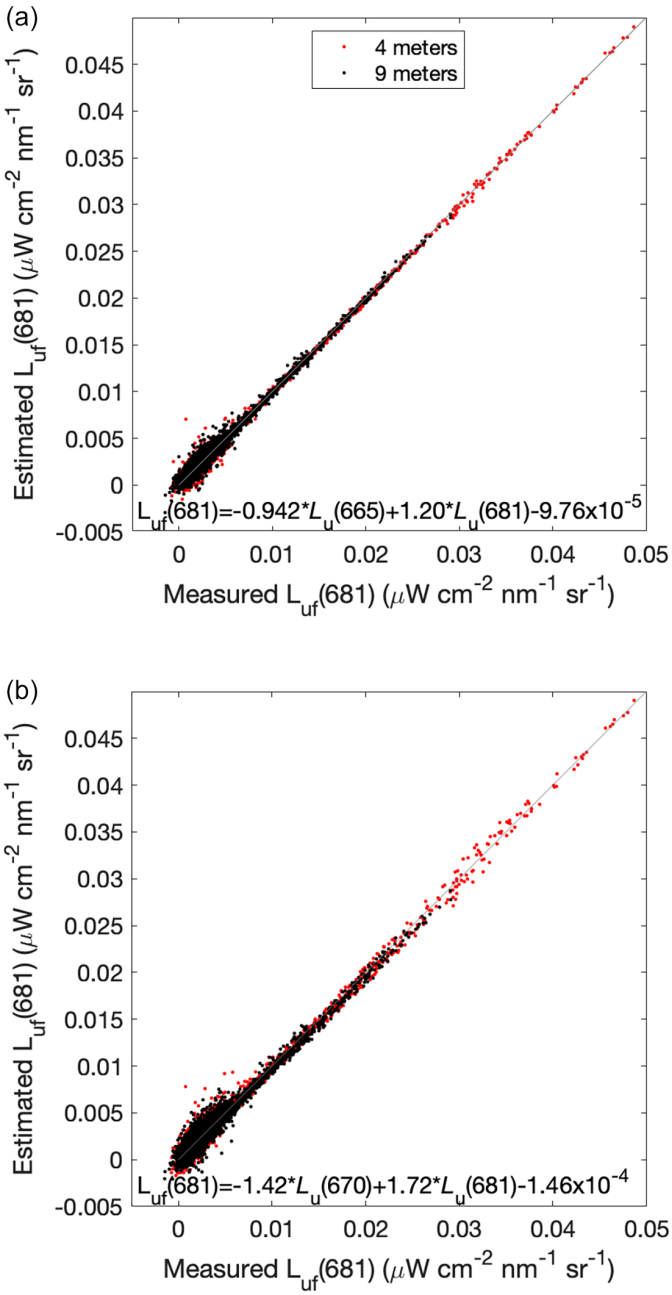

Fig. 2. Measured L_{uf} (681) obtained from the line height approach from hyperspectral radiometers and L_{uf} (681) estimated using a linear function of (**a**) L_u(665) and L_u(681) and (**b**) L_u(670) and L_u(681). The equation is provided in each panel. The color of the dots is for the two different depths of measurements. Variability in the lower values arise primarily from the lower sensitivity of the hyperspectral sensors in the red bands.

organic matter on the quantum yield retrievals. Both algorithms are expected to provide similar results in waters where variations in the ratio of absorption by colored dissolved organic matter to chlorophyll follow statistical trends with trophic state (chlorophyll concentration).

Average mixed layer irradiance

The average $E_d(490)$ irradiance in the mixed layer was calculated as

$$E_{MLD} = \frac{1}{z_{MLD}} \int_0^{z_{MLD}} E_d(490,4) e^{-K_d(490)(z-4)} dz \quad (1)$$

where z_{MLD} (m) is the climatological mixed layer depth (Houpert et al. 2015), $E_d(490,4)$ is the mean daily irradiance at 4 m, $K_d(490)$ is the diffuse attenuation coefficient for downward irradiance at 490 nm (m^{-1}) calculated from the measured $E_d(490)$ at 4 and 9 m on the mooring. Note that using climatological data allows the average phenology of the mixed layer depth to be accounted for but prevents assessing their impact at yearly or shorter timescales.

Fluorescence model

Sun-induced fluorescence

To interpret the $L_{uf}^{E,F}(681,z,t)$ vs. $E_d(490, z)$ curves we used a model that describes its variation in terms of key parameters (e.g., Morrison 2003; Schallenberg et al. 2008). In this model, the absorption by photosynthetic pigments associated with photosystem II (the relevant measure of concentration/biomass for fluorescence studies) is assumed constant for the day. The model uses 6 parameters (*see* Fig. 3) and is inspired by the work of Ru Morrison (2003; 2010). It separates two parts: (1) the basal fluorescence and photochemical quenching (F_{PQ}, sr^{-1}) and (2) the non-photochemical quenching (f_{NPQ}, non-dimensional). The full model is obtained by multiplying both parts: $L_{uf}^{E,F}(681,z,t) = F_{PQ}(t) f_{NPQ}(t)$. The depth dependence is dropped from the notation of the left side to lighten it, but fits are carried out for each depth separately. The model is described as a function of $E_d(490, t)$ which is assumed representative of the variations in photosynthetically usable radiation (PUR; e.g., Morel 1978). We assume that an irradiance above which NPQ is initiated exists (E_{d0NPQ}, $\mu W\ cm^{-2}\ nm^{-1}$) and that below this irradiance $f_{NPQ} = 1$. We also assume that above this irradiance the fraction of reaction centers that are closed remains constant (i.e., F_{PQ} is constant and equal to its value at E_{d0NPQ} for all $E_d(490) > E_{d0NPQ}$). Below and above E_{d0NPQ}, the fluorescence response of both F_{PQ} and f_{NPQ} are treated differently. For f_{NPQ}: (1) we define the non-photochemical quenching amplitude (A_{NPQ}), which has values between 0 (for no quenching) and 1 (for complete quenching) and (2) a "saturation irradiance for NPQ" (E_{kNPQ}, $\mu W\ cm^{-2}\ nm^{-1}$) that is an irradiance value above E_{d0NPQ} where $L_{uf}^{E,F}(681,z,t)$ has decreased by 63% from its maximum. Minimum ($L_{uf\ min}^{E,F}$) and maximum ($L_{uf\ max}^{E,F}$) values are fitted to the measured $L_{uf}^{E,F}(681,z,t)$ values as well as a parameter representing the saturation of fluorescence at low light (E_{kPQ}).

For $E_d(490, t) < E_{d0NPQ}$:

$$F_{PQ}(t) = L_{uf\ min}^{E,F} + \left(L_{uf\ max}^{E,F} - L_{uf\ min}^{E,F}\right)\left(1 - e^{-\frac{E_d(490,t)}{E_{kPQ}}}\right) \text{ and } f_{NPQ}(t) = 1 \quad (2a)$$

For $E_d(490, t) > E_{d0NPQ}$:

$$F_{PQ}(t) = L_{uf\ min}^{E,F} + \left(L_{uf\ max}^{E,F} - L_{uf\ min}^{E,F}\right)\left(1 - e^{-\frac{E_d(490,t)}{E_{kPQ}}}\right) \text{ and } f_{NPQ}(t) = 1 - A_{NPQ}\frac{1 - e^{\left(-\frac{\left[E_d(490,t) - E_{d0NPQ}\right]}{E_{kNPQ}}\right)}}{1 - e^{\left(-\frac{\left[E_{dmax}(490) - E_{d0NPQ}\right]}{E_{kNPQ}}\right)}} \quad (2b)$$

where $E_{dmax}(490)$ is the maximum irradiance for the day over which the function is fitted.

Active fluorometer

The active fluorometer data is fitted to a similar model. However, because the measuring light is saturating, F_{PQ} is not light dependent. For this reason, the model is simplified by setting the $\left(1 - e^{-E_{d0NPQ}/E_{kPQ}}\right) = 1$ (i.e., assuming all reaction centers are closed) and therefore $F_{PQ} = F_{max}$. The fluorescence model becomes $F = F_{max} f_{NPQ}$ with f_{NPQ} taking the same form as above, where F is the fluorescence measured by the active fluorometer.

Estimation of parameters

A bounded reflexive non-linear least-square approach (Coleman and Li 1996) was used to obtain the parameters with irradiance and $L_{uf}^{E,F}(681,z,t)$ or F as input variables. It was found that the minimum fousquare root error was dependent on the initial guess as the algorithm could identify local minima. A comparison with two global search algorithms in Matlab 2019a referred to as *Particle swarm algorithm* (Eberhart and Kennedy 1995; Pedersen 2010; Mezura-Montes and Coello Coello 2011) and *Global Search* (Ugray et al. 2007) applied with a sum of squared errors objective function showed that with starting points (initial guesses) that are chosen close the expected yearly mean values for each parameter, the retrieved parameters from the bounded reflexive non-linear least-square approach are very close to the global search algorithms and yearly patterns are essentially identical.

Interpretation of the estimated parameters

The parameters estimated can be interpreted as follow (*see* Fig. 3):

1. $L_{uf\ min}^{E,F}$ is the intercept of the $L_{uf}^{E,F}(681,z,t)$ vs. $E_d(490, z)$ curve;
2. $L_{uf\ max}^{E,F}$, F_{max}, are the hypothetical maximum value of $L_{uf}^{E,F}$ and active fluorescence respectively measured without NPQ;

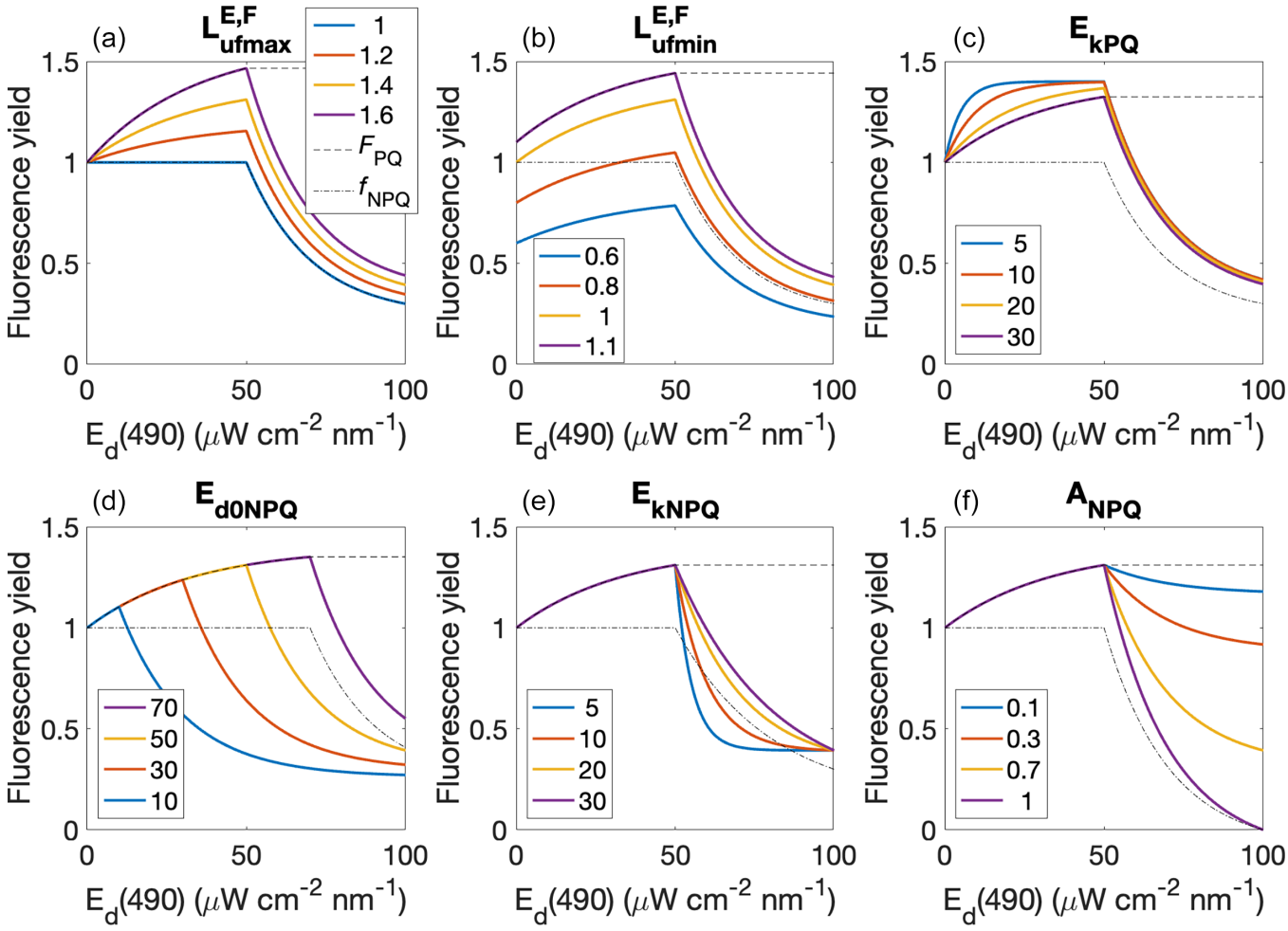

Fig. 3. Impact of varying the parameters in the passive fluorescence model (Eqs. 2a and 2b) on the shape of the fluorescence quantum yield vs. $E_d(490)$. In each panel, four values (in legend) of the parameter in the title are shown along with the F_{PQ} and f_{NPQ} function for the purple line (*see* panel **a** for legend). The pale orange line (i.e., legend in panel a = 1.4) is repeated in each panel and provides a reference. For the active fluorescence model, the photochemical quenching part is not present and its shape becomes the same as the f_{NPQ} line with the maximum being F_{max} (i.e., the dash-dot line in all panels—superposed to blue line in panel—is the active model equivalent to the passive model purple line).

3. E_{d0NPQ} is the $E_d(490, z)$ at which non-photochemical quenching is initiated;
4. A_{NPQ} is the amplitude of the non-photochemical quenching at the maximum irradiance measured that day at the depth of the measurement (4 or 9 m). It represents a multiplicative fraction of $L^{E,F}_{uf\,max}$ or F_{max} ($A_{NPQ}L^{E,F}_{uf\,max}$ or $A_{NPQ}F_{max}$) such that when $A_{NPQ} = 1$, fluorescence is not reduced from $L^{E,F}_{uf\,max}$ or F_{max} by non-photochemical quenching and when $A_{NPQ} = 0$, fluorescence is reduced to 0;
5. E_{kPQ}, is the irradiance at which fluorescence is 63% of the maximum it would reach if there was no non-photochemical quenching. It is related to the initial slope of the curve by the following expression: $\alpha_f = \frac{L^{E,F}_{uf\,max} - L^{E,F}_{uf\,min}}{E_{kPQ}}$;
6. E_{kNPQ} the irradiance above E_{d0NPQ} where the fluorescence has decreased to 36.7% of the difference between $L^{E,F}_{uf\,max}$ and $A_{NPQ}L^{E,F}_{uf\,max}$ or F_{max} and $A_{NPQ}F_{max}$. If E_{d0NPQ} is 50 μW cm^{-2} nm^{-1} sr^{-1} and E_{kNPQ} is 5 μW cm^{-2} nm^{-1} sr^{-1}, then 36.7% of the difference is reached at 55 μW cm^{-2} nm^{-1} sr^{-1};
7. $E_{dmax}(490)$ is the maximum irradiance during the day at each depth.

Results

$L^{E,F}_{uf}$ and F_{max} follow primarily the large changes in phytoplankton abundance (Fig. 4), with maxima during the spring bloom followed by lower values in summer and a slow increase throughout the fall. This highlights that $L^{E,F}_{uf}$ and F_{max} reflect the total emission of fluorescence not the quantum yield (i.e., only the intraday variation can be interpreted in terms of changes in the quantum yield). We note parenthetically, because it is beyond the scope of this paper to examine details of the biomass phenology, that the increase in biomass in the fall (fluorescence is used as a proxy), which continues

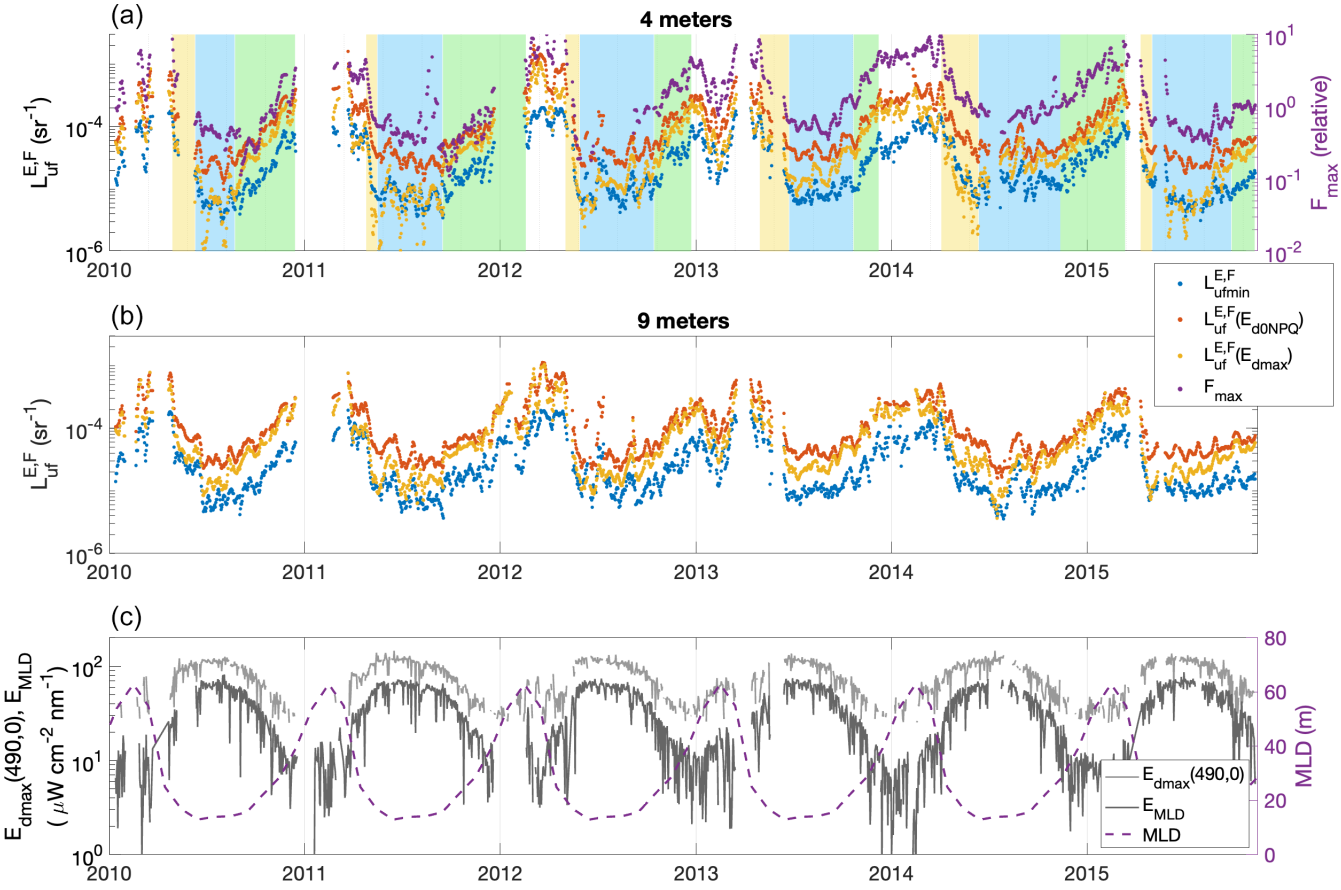

Fig. 4. Amplitude of the Sun-induced fluorescence at (**a**) 4 m and (**b**) 9 m, and (**c**) the incident irradiance at the surface, the average irradiance in the mixed layer (left axis) and the inferred mixed layer depth climatology (right axis). In panel a, the F_{max} parameter from the active fluorometer sensor is also plotted (scaled). Background is colored according to phytoplankton abundance dynamics: yellow for spring bloom termination (likely nutrient starvation; identified as the period of decreasing fluorescence following the yearly maximum), blue for low chlorophyll summer stratified (nutrient limitation; identified as a more or less constant and low phytoplankton abundance period in summer), and green for slow net growth initiation of spring bloom (light limitation; identified as a period of increasing fluorescence following the summer period up to the plateau or maximum in the spring).

unabated until the spring bloom (though sometimes with a decrease in February, *see* Fig. 4b in 2012 and 2013), is initiated with the deepening of the mixed layer and is therefore inconsistent with Sverdrup critical depth hypothesis and the timing is more consistent with the disturbance-recovery hypothesis (Behrenfeld and Boss 2014). This relationship with phytoplankton abundance is observed at different positions on the $L_{uf}^{E,F}$ vs. $E_d(490)$ curve (i.e., all variables in Fig. 4a,b): the y intercept ($L_{ufmin}^{E,F}$), the maximum of the fitted curve when NPQ is initiated ($L_{uf}^{E,F}(E_{d0NPQ})$) and at the maximum irradiance during the day (generally when NPQ is maximum) $L_{uf}^{E,F}(E_{dmax}(490))$. Both at 4 and 9 m, while $L_{uf}^{E,F}(E_{d0NPQ})$ is, by definition, the highest value, $L_{uf}^{E,F}(E_{dmax}(490))$ tends to be closer to $L_{ufmin}^{E,F}$ after the bloom termination and into the summer at 4 m (section with blue background on Fig. 4) and closer to $L_{uf}^{E,F}(E_{d0NPQ})$ during the higher phytoplankton abundance and lower irradiance period reflecting lower non-photochemical quenching (*see* also Fig. S1D showing consistent trends in the A_{NPQ} parameter). The maximum fluorescence measured by the fluorometer (F_{max}) at 4 m follows closely the patterns of $L_{ufmin}^{E,F}$ and $L_{uf}^{E,F}(E_{d0NPQ})$.

While $L_{ufmin}^{E,F}$ are very similar at 4 and 9 m (Fig. 5a) in all months, reflecting uniform phytoplankton concentration within the top 10 m (more precisely photosynthetic pigment absorption), $L_{uf}^{E,F}(E_{dmax}(490))$ tends to be higher at 9 m than at 4 m (Fig. 5b) particularly between May and July. This reflects the stronger non-photochemical quenching nearer to the surface at that time.

All retrieved photophysiological parameters from the least-square estimates show clear annual patterns with generally higher values in the summer months (Fig. 6; *see* also Fig. S1). These patterns are very similar whether they are measured using the active fluorometer (F[4] in Fig. 6) or the upwelling radiance from Sun-induced fluorescence (and using morning or afternoon fits, *see* Fig. S2). Two key differences are notable, however. The first occurs in the E_{d0NPQ} parameter whereby the values are smaller than the values retrieved with the Sun-induced fluorescence in fall and winter. The second is the fall

(and winter) values of the A_{NPQ} from the fluorometer which are generally (except in 2014; *see* Fig. S1) much higher than the Sun-induced values. We do not have an explanation for these differences. The A_{NPQ} values from the fluorometer are also less variable throughout the year. Although this reduced variability may be more a reflection of averaging years with high values and years with low values rather than more even data throughout the year (*see* Fig. S1). These opposite differences for active A_{NPQ} and E_{d0NPQ} compared to Sun-induced fluorescence are the result of the similar, albeit noisy, E_{kNPQ} retrieved for active vs. Sun-induced fluorescence (at the same E_{kNPQ}, when A_{NPQ} goes up, E_{d0NPQ} must come down and vice versa). There is also limited differences between depths in the retrieved parameters from the $L_{uf}^{E,F}$ measurements, except for A_{NPQ} which shows higher values (more non-photochemical quenching) at 4 m than at 9 m particularly during the months with the highest irradiance (coherent with the observations on Fig. 5).

When grouped by growth irradiance, the most noticeable difference in shape of the $L_{uf}^{E,F}$ vs. $E_d(490)$ curves are decreasing initial slopes with increasing growth irradiance which leads to a shift in the position of the maximum fluorescence toward higher irradiance values (Fig. 7a). Another noticeable feature of these curves are the remarkably similar decreasing slopes beyond $E_{dmax}(490)$ across all growth irradiances (Fig. 7a). The ratio between maximum and minimum $L_{uf}^{E,F}$ is also very constant (Fig. 7a). When looking at the different phenological periods, similar results are observed. The only noticeable systematic differences in shape of the $L_{uf}^{E,F}$ vs. $E_d(490)$ is during what we refer to as the "light limited" growth period, which is mostly the fall period where the phytoplankton abundance is increasing and there is likely very little nutrient limitation. During this period, there is a marked shift in the difference between the minimum and maximum $L_{uf}^{E,F}$ which increased with growth irradiance. This also leads to a shift in the position of the maximum toward higher $E_{dmax}(490)$, but with very little changes in the initial slope of the curve, which appear to be near the highest values of the year. Large changes in the phytoplankton communities occur at the BOUSSOLE site throughout the year (*see* e.g., Organelli et al. 2013) with a spring bloom dominated by diatoms and haptophyte and the summer and fall dominated by picoplankton and haptophytes (inferred as pico-phytoplankton and nanophytoplankton from HPLC). While communities adapt differently to growth irradiance and have different optical characteristics (e.g., Morel and Bricaud 1981), different attempts to relate the extracted parameters to HPLC-derived community composition did not provide convincing results.

One intriguing aspect of these curves is the large ratio of maximum to initial value of the curve. If we were to calculate a F_v/F_m with these curve, where $F_v = F_m - F_0$ and F_0 is the minimum fluorescence, it would be around 0.75–0.8, which is much higher than the single turnover (or DCMU based) F_v/F_m that are measured on cultures (Suggett et al. 2009). Part of the explanation may lie in the measurement being closer to a multiple turnover rate measurement for F_m which are significantly higher than the single turnover rate estimates (Kromkamp and Forster 2003); or the narrow waveband measured by the radiometer near 681 nm, which leads to the higher F_v/F_m than observed with a broad emission band used in many fluorometers (e.g., Simis et al. 2012). Finally, growth

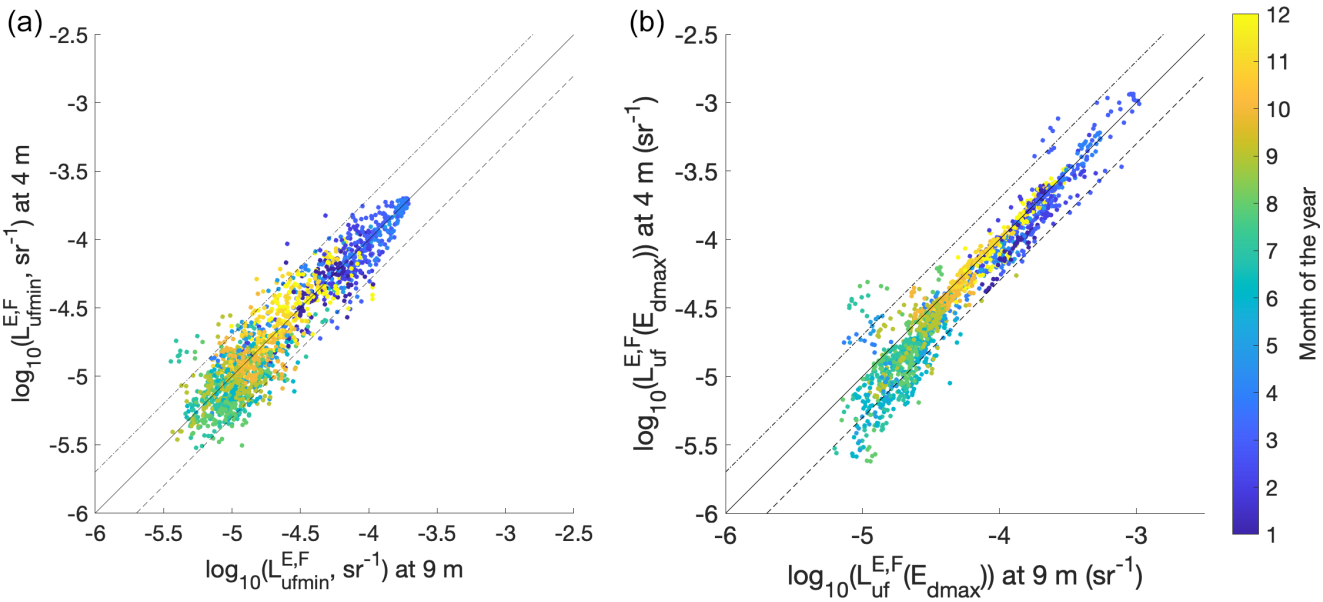

Fig. 5. Comparison of the upwelling fluorescence radiance at 4 and 9 m for (**a**) $L_{uf\,min}^{E,F}$ and (**b**) the L_{uf} at the maximum daily irradiance. Solid line is 1 : 1, while the two dashed lines are 0.5 : 1 and 2 : 1.

is another likely explanation that could partly explain this observation.

The MODIS measurements at the BOUSSOLE site (Fig. 8) are consistent with the in-situ data. The overall nflh follows the chlorophyll *a* measurement as expected and the nflh patterns are also very similar to the in-situ measurement of $L_{uf}^{E,F}$ (compare Fig. 8 with Fig. 4). The retrieved quantum yields using two algorithms show very similar patterns and are highly variable. Much of this variability appears on a timescale of a few days to weeks, with some variability occurring at seasonal timescales. The seasonal patterns, however, are not repeatable from year to year such that no phenology is observed, unlike what is observed in the photophysiological parameters.

Discussion

Variability in the quantum yield of fluorescence arises from multiple sources that interact together (*see* the following papers and references therein Loftus and Seliger 1975; Laney, Letelier, and Abbott 2005; Huot and Babin 2010; Lin et al. 2016). These include the molecular structure of photosystem II antenna, species composition, light environment, nutrient availability and hydrodynamics of the surface layer. These can all potentially affect the maximum quantum yield of the cell and its photochemical and non-photochemical quenching capacities. From a modeling perspective this is an intractable problem or at least one that cannot be constrained. In addition, except for lifetime measurements of the quantum yield (e.g., Lin et al. 2016), most measurements are *apparent* quantum yield which include variability from the ratio of photosystem II photosynthetic pigments (contributing to fluorescence) to all other pigments in the cell (non-photosynthetic and photosystem I). Finally, the observed quantum yields obtained from radiometry include the impact of intracellular optical effects (absorption efficiency and reabsorption of emission within the cell). While all these can be corrected for, in principle, in most cases we only have statistical relationship to make these corrections (e.g., trend with trophic status expressed as chlorophyll). The measured quantum yield from in situ radiometers also include the errors from the measurement of fluorescence and in the variables used to retrieve the yield. Those same errors are present and larger in remote sensing estimates due to the difficulty of measuring the water leaving radiance from fluorescence especially in low chlorophyll waters where the signal is very small (Abbott and Letelier 1999; Huot, Franz, and Fradette 2013; Lin et al. 2016). Faced with this problem to use the quantum yield of fluorescence measured from satellite radiometers, we must verify which of the above source(s) of variance are the largest or dominant source of variance in our study region and period for our measurement (morning, midday, time resolved) and then, and only then, the fluorescence measurement can be used to obtain information about that source of variability. In the case of the quantum yields measured from MODIS in

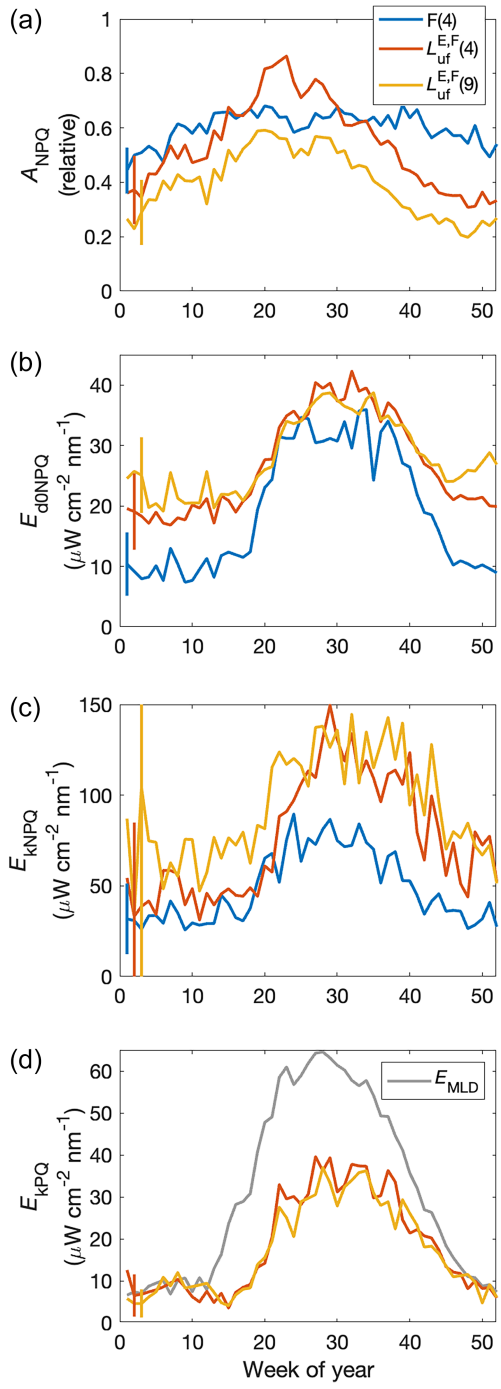

Fig. 6. Weekly averages over the time series of (**a**) A_{NPQ}, (**b**) E_{d0NPQ}, (**c**) E_{kNPQ}, (**d**) E_{kPQ}, for the upwelling fluorescence radiance ($L_{uf}^{E,F}$) at 4 and 9 m, and the active fluorescence (except in d as E_{kPQ} is not retrieved from the active fluorescence model). The retrieved parameters are the average of the morning and afternoon fits (very little difference exist between morning and afternoon retrieved parameters; Fig. S2). The average mixed layer depth irradiance is presented (μW cm^{-2} nm^{-1}) in panel d. For panel a–c, ± 1 standard deviation from the mean of week 1 for $F(4)$, week 2 for $L_{uf}^{E,F}(4)$, week 3 $L_{uf}^{E,F}(9)$ are presented as vertical lines to provide an indication of the variability in the data (*see* also Fig. S1).

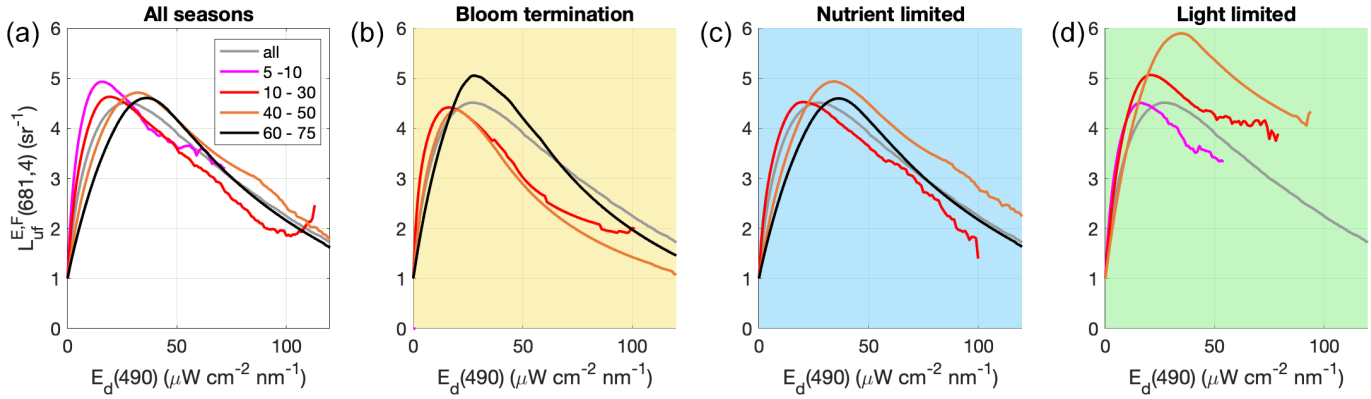

Fig. 7. Average values of the fit of the $L_{uf}^{E,F}$ vs. $E_d(490)$ curves normalized to $L_{uf\ min}^{E,F}$ for all seasons together (**a**) as well as different periods of the phenology (**b**–**d**) for different growth irradiance (line colors) estimated as the average irradiance in the mixed layer. The background colors refer to the same colors as on Fig. 4, except for the first panel which includes the whole time series and not only the white sections of Fig. 4.

Fig. 8, we do not have currently any information that helps us identify the main source of variability in the time series.

In this paper by using measurements made over 1 d (the analysis returns essentially the same result using only half days) and using only the relative changes in the signal it means that the extracted variables are not affected by the amplitude of the fluorescence signal (e.g., chlorophyll concentration). By doing this we largely avoid many sources of variability in the signal that are present in typical radiometry: errors in phytoplankton absorption estimates, errors in optical properties of the water, errors in geometry (e.g., bidirectional reflectance correction for satellite measurements). By using relative daily changes (and

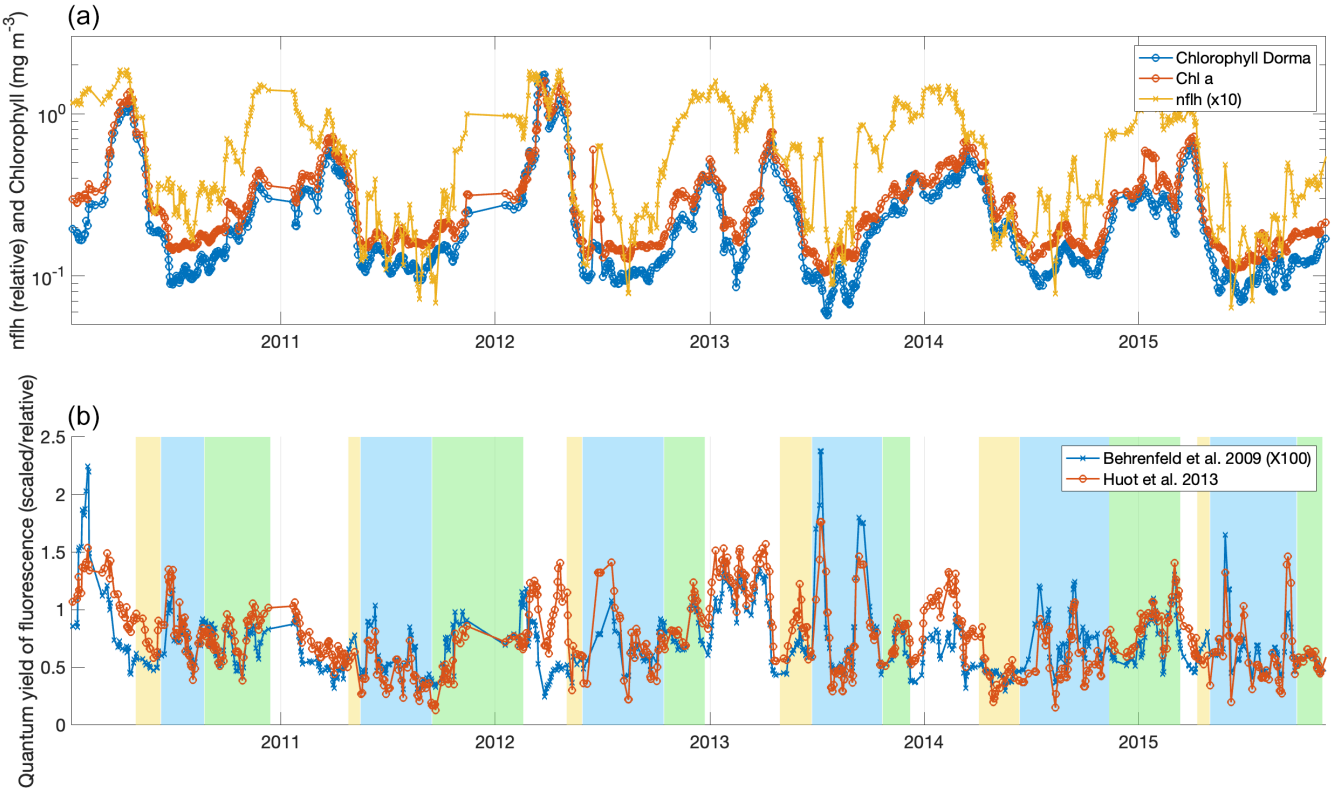

Fig. 8. MODIS measurements at the BOUSSOLE site. (**a**) Chlorophyll concentration using the L-Dorma algorithm tuned for the Mediterranean Sea (blue line) and the standard MODIS algorithm (red). (**b**) Two estimates of the quantum yield of fluorescence from the algorithms proposed by Behrenfeld et al. (2009) and Huot, Franz, and Fradette (2013). All data are the mean from a 5 × 5 pixel square centered on the BOUSSOLE site and were smoothed using a 9-point running average.

assuming constancy in these properties over half a day), we also avoid sources of variability related to the optical characteristics of the cell (absorption efficiency and reabsorption) and the potentially changing values of the maximum quantum yield of fluorescence. Finally, the changes observed reflect those of the true quantum yield and not the apparent quantum yield as we do not have to use an absorption coefficient to obtain estimates of the quantum yield. In essence, by never measuring the quantum yield, but only its relative changes, we avoid many of the pitfalls associated with the measurement of the absolute value of the quantum yield and its interpretation. It is therefore not surprizing that the patterns obtained from MODIS in Fig. 8 do not follow our retrieved parameters.

The resulting patterns in the extracted parameters obtained both from in situ active fluorometry and from Sun-induced fluorescence show strong seasonal patterns that are clearly linked to photoadaptation and photoacclimation of phytoplankton to the growth irradiance. These patterns show a strong phenology and respond as expected from in situ and laboratory studies for those that are well understood such as the saturation irradiance of photochemistry. This shows a strong potential for measurement of fluorescence at high temporal resolution using simple fluorometers or radiometers to provide physiological information on phytoplankton from autonomous mooring and eventually from geostationary satellites or trains of Sun-synchronous low-Earth orbit ocean color satellites. In the following, we explore more closely each aspect of this potential.

As mentioned above, the theoretical model used herein is inspired by the model developed by Morrison (2003). In his original description Morrison used the model to interpret profiles of Sun-induced fluorescence. Assuming uniform phytoplankton photoacclimation and photoadaptation, the model fit well the measured profiles and was able to retrieve the parameters for several profiles by inversion. A similar model was then used by Schallenberg et al. (2008) on a 3-month time series of measurements of Sun-induced fluorescence by autonomous profiling floats. Higher fluorescence yields, which varied on a weekly timescale, were interpreted in terms of increased nutrient stress to surface waters. This is, to our knowledge, the only application of this type of model to time series of Sun-induced fluorescence.

The suggestion that Sun-induced fluorescence could be used to estimate primary production has largely been based on the potential existence of a simple relationship between the quantum yields of carbon fixation and of fluorescence (Kiefer, Chamberlin, and Booth 1989; Chamberlin et al. 1990; Chamberlin and Marra 1992). Such suggestions were made before we had a good understanding of non-photochemical quenching. In reality, however, there is no simple relationship between Sun-induced fluorescence quantum yield and photosynthetic quantum yields (Kolber and Falkowski 1993). This does not mean that they cannot be useful toward improving estimates of primary production. The parameters derived herein may offer new possibilities to obtain information about photosynthetic processes. For example, E_{kPQ} should vary with the light saturation parameter of photosynthesis vs. irradiance curves, E_k. Furthermore, it can be shown (*see* Supporting Information) that the initial slope of the curve presented in Fig. 7 (i.e., when the $L_{uf}^{E,F}$ curve is normalized to the value at $L_{uf\,min}^{E,F}$) is directly linked to key photophysiological parameters. Specifically, it is equal to $\frac{\varphi_{Po}^{max}}{E_{kPSII}\,\varphi_{No}}$ where E_{kPSII} is the saturation irradiance for the electron transport through PSII (i.e., same as oxygen evolution), φ_{Po}^{max} is the maximum quantum yield of charge separation and φ_{No} is the basal quantum yield of non-photochemical processes (i.e., sum of fluorescence and heat) in dark regulated PSII. Such mechanistic links are much harder to derive at higher irradiance or would require several assumptions that may not be warranted. Empirical relationships may, however, exist but will require extensive datasets of simultaneous measurements of fluorescence (ideally including fast repetition rate fluorometry or similar instrumentation) and carbon fixation. One such example was derived by Comeau (2010) where he showed a strong relationship between the saturation parameter of photosynthesis for carbon fixation and $L_{uf}^{E,F}\left(E_{d0NPQ}\right)$ (his "EFT" parameter). Some of the particularly intriguing parameters to explore are difference ratios using $L_{ufmin}^{E,F}$ and $L_{uf}^{E,F}\left(E_{d0NPQ}\right)$ and different measures of NPQ.

In addition to $E_{k,}$ a critical parameter for estimating primary production (scaling all estimates) at sea is the maximum rate of photosynthesis in light saturated conditions (i.e., P_{max} or its biomass normalized version P_{max}^{B}) (Ryther and Yentsch 1957; Platt and Sathyendranath 1993; Antoine, André, and Morel 1996). This parameter is also the most difficult to constrain on large spatial scales and through time, and many parameterizations that rely on remotely observable proxies (usually chlorophyll, temperature, or irradiance) have been proposed (Ryther and Yentsch 1957; Platt and Sathyendranath 1993; Antoine, André, and Morel 1996). The parameters derived above from fluorescence are directly linked to photoacclimation and photoadaptation and are therefore excellent candidates for future parameterization of P_{max} which could, for example, use traditional variables as well as one or some of these new parameters in a multivariate statistical model. However, these parameters are not yet obtainable at such large scales and would require remote sensing measurements with a high temporal resolution ($\sim$15 min) with clear skies for at least half a day including low light periods (morning or evening). This is not currently possible even with current geostationary satellite (e.g., O'Malley and Behrenfeld 2014).

The GOCI satellite has been used by O'Malley and Behrenfeld (2014) to study changes in the shape of the fluorescence vs. irradiance curve. To infer photoacclimation state they used a theoretical model (their fig. 1 and associated text) that describes the changing shape of the fluorescence vs. irradiance curve as a function of growth irradiance. For phytoplankton acclimated to

lower growth irradiance the modeled curve has two key characteristics, a steeper initial slope (i.e., a lower E_k) and a greater rate of decrease after the maximum leading to lower fluorescence yield at high irradiance due to non-photochemical quenching. The former is consistent with our observation at the BOUSSOLE site, whereas the second is not as we do not see strong variation in the slope of non-photochemical quenching (*see* Fig. 7). The signal-to-noise ratio of the GOCI sensor is not sufficient at low light to obtain reliable estimates of Sun-induced fluorescence (O'Malley and Behrenfeld 2014) and therefore they had to use the high light portion of the fluorescence vs. irradiance curve for their retrievals. Apart from the different areas of studies (and associated nutrient limitations, species composition, etc.), we do not have an explanation for this discrepancy, however, phytoplankton at BOUSSOLE do not seem to follow this theoretical model at high light. What is clear, however, is that, in their current form, geostationary satellites may not allow obtaining Sun-induced fluorescence parameters estimates that provide insights into photophysiology. Only much higher signal to noise ratios would allow collecting information on the light-limited portion of the curve.

The MODIS quantum yield estimates have been used in the past to infer iron limitation at large scales (Behrenfeld et al. 2009; Browning, Bouman, and Moore 2014; Browning et al. 2023). Iron limitation as a main source of variability in regions with sufficient fluorescence emission (i.e., high phytoplankton absorption coefficient) is also supported to some extent by in situ lifetime measurements (Lin et al. 2016). At the BOUSSOLE site, iron limitation is not expected due to significant atmospheric inputs of iron (Heimbürger, Migon, and Cossa 2011). The observed changes in the quantum yield of fluorescence (Fig. 8) do not reflect any of the retrieved parameters from the fluorescence model. The time series of the MODIS quantum yield of Sun-induced fluorescence collected near noon and therefore provides little, if any, information about the changes in phytoplankton photoacclimation or photoadaptation. This contrast with the findings of Morrison and Goodwin (2010) who suggest that photoacclimation and photoadaptation were responsible for most of the variance in the quantum yield of fluorescence in the Gulf of Maine. To arrive at this conclusion, they had to use a series of assumptions regarding the maximum quantum yield of fluorescence and "photoinhibition"-related non-photochemical quenching (*see* details in their supporting information) to obtain their "E_T" parameter (akin to our E_{kNPQ}). These assumptions likely led to the E_T showing an inverse relationship with growth irradiance and leading to their conclusions. These assumptions were not required here as we had access to timeseries with high temporal resolution. Future studies looking at short term changes (e.g., Schallenberg et al. 2008) in the MODIS signal may allow interpretation of the variability observed at these scales.

To conclude, it is easy to be enthusiastic about the potential of Sun-induced fluorescence to support ocean research and monitoring or to overinterpret the results. In the case of the results described above, to verify the potential and turning it to operational opportunities, we can dream of autonomous in situ observations systems that are instrumented to assess at high temporal resolution the photophysiology (e.g., fast repetition rate fluorometers), species composition (e.g., imaging flow cytometer), together with spectrometers to obtain Sun-induced fluorescence. Combining this with regular cruises measuring carbon fixation (P vs. E curves) would likely provide the necessary data to fully understand the use of the parameters retrieved here. If you allow us to indulge in our daydreaming a little further, we imagine a train of small ocean color observing satellites, say 10–15 during a day, that had variable spatial and radiometric resolution allowing to capture the full daily changes in the water leaving fluorescence radiance.

Author Contributions

Yannick Huot: Conceptualization (equal), Formal Analysis (lead), Methodology, Writing – Original Draft Preparation (lead); Investigation (equal). David Antoine: Conceptualization (equal), Validation (equal); Funding Acquisition (lead), Methodology (equal), Writing – Review & Editing (equal), Project Administration (lead); Investigation (equal). Vincenzo Vellucci: Data Curation (lead); Validation (equal); Funding Acquisition (co-lead), Investigation (equal); Writing – Review & Editing (equal).

Acknowledgments

We thank two reviewers for their constructive and thorough reviews which have contributed to improve the paper. This research was supported through the Canada Research Chair and NSERC discovery grant programs (Yannick Huot). The BOUSSOLE project was funded by the Centre National d'Etudes Spatiales (CNES) and the European Space Agency (ESA ESRIN, contract no. 4000119096/17/I-BG), with staff support from the Institut National des Sciences de l'Univers of the Centre National de la Recherche Scientifique (CNRS-INSU) and Sorbonne Université, and ship time from the French Oceanographic Fleet (FOF).

Conflicts of Interest

David Antoine is associate editor at Limnology and Oceanography.

References

Abbott, M. R., and R. M. Letelier. 1999. MODIS ATBD No. 22 Chlorophyll Fluorescence. 1996.

Antoine, D., J. M. André, and A. Morel. 1996. "Oceanic Primary Production 2. Estimation at Global Scale From Satellite (Coastal Zone Color Scanner) Chlorophyll." *Global*

Biogeochemical Cycles 10: 57–69. https://doi.org/10.1029/95GB02832.

Antoine, D., M. Chami, H. Claustre, F. d'Ortenzio, and A. Morel. 2006. BOUSSOLE: A Joint CNRS-INSU, ESA, CNES, and NASA Ocean Color Calibration and Validation Activity, 214147. Greenbelt, Maryland: NASA. https://ntrs.nasa.gov/citations/20070028812

Antoine, D., V. Vellucci, A. C. Banks, et al. 2020. "ROSACE: A Proposed European Design for the Copernicus Ocean Colour System Vicarious Calibration Infrastructure." *Remote Sensing* 12: 1535. https://doi.org/10.3390/rs12101535.

Behrenfeld, M. J., and E. S. Boss. 2014. "Resurrecting the Ecological Underpinnings of Ocean Plankton Blooms." *Annual Review of Marine Science* 6: 167–194. https://doi.org/10.1146/annurev-marine-052913-021325.

Behrenfeld, M. J., T. K. Westberry, E. S. Boss, et al. 2009. "Satellite-Detected Fluorescence Reveals Global Physiology of Ocean Phytoplankton." *Biogeosciences* 6: 779–794. https://doi.org/10.5194/bg-6-779-2009.

Browning, T. J., H. A. Bouman, and C. M. Moore. 2014. "Satellite-Detected Fluorescence: Decoupling Nonphotochemical Quenching From Iron Stress Signals in the South Atlantic and Southern Ocean." *Global Biogeochemical Cycles* 28: 2013GB004773. https://doi.org/10.1002/2013GB004773.

Browning, T. J., M. A. Saito, S. P. Garaba, et al. 2023. "Persistent Equatorial Pacific Iron Limitation Under ENSO Forcing." *Nature* 621: 330–335. https://doi.org/10.1038/s41586-023-06439-0.

Chamberlin, S., and J. Marra. 1992. "Estimation of Photosynthetic Rate From Measurements of Natural Fluorescence: Analysis of the Effects of Light and Temperature." *Deep Sea Research* 39: 1695–1706. https://doi.org/10.1016/0198-0149(92)90024-N.

Chamberlin, W. S., C. R. Booth, D. A. Kieffer, J. H. Morrow, and R. C. Murphy. 1990. "Evidence for a Simple Relationship between Natural Fluorescence, Photosynthesis and Chlorophyll in the Sea." *Deep Sea Research Part A. Oceanographic Research Papers* 37: 951–973. https://doi.org/10.1016/0198-0149(90)90105-5.

Coleman, T. F., and Y. Li. 1996. "An Interior, Trust Region Approach for Nonlinear Minimization Subjects to Bounds." *SIAM Journal on Optimization* 6: 418–445. https://doi.org/10.1137/0806023.

Comeau, A. J. 2010. "Examining Temporal Variations of Phytoplankton Photoacclimation Using a Novel Fluorescence Based Approach." https://doi.org/10.1021/jm100528p.M. Sc., Dalhousie University.

D'Ortenzio, F., S. Marullo, M. Ragni, M. Ribera d'Alcalà, and R. Santoleri. 2002. "Validation of Empirical SeaWiFS Algorithms for Chlorophyll-*a* Retrieval in the Mediterranean Sea: A Case Study for Oligotrophic Seas." *Remote Sensing of Environment* 82: 79–94. https://doi.org/10.1016/S0034-4257(02)00026-3.

Eberhart, R., and J. Kennedy. 1995. "Particle Swarm Optimization." In Proceedings of the IEEE International Conference on Neural Networks, 1942–1948. New York: Citeseer.

Falkowski, P. G., and Z. Kolber. 1995. "Variations in Chlorophyll Fluorescence Yields in Phytoplankton in the World Oceans." *Australian Journal of Plant Physiology* 22: 341–355. https://doi.org/10.1071/PP9950341

Geider, R. G., H. L. L. MacIntyre, and T. M. Kana. 1996. "A Dynamic Model of Photoadaptation in Phytoplankton." *Limonology and Oceanography* 41: 1–15. https://doi.org/10.4319/LO.1996.41.1.0001

Han, B. P. 2001. "Photosynthesis-Irradiance Response at Physiological Level: A Mechanistic Model." *Journal of Theoretical Biology* 213: 121–127. https://doi.org/10.1006/jtbi.2001.2413.

Heimbürger, L.-E., C. Migon, and D. Cossa. 2011. "Impact of Atmospheric Deposition of Anthropogenic and Natural Trace Metals on Northwestern Mediterranean Surface Waters: A Box Model Assessment." *Environmental Pollution* 159: 1629–1634. https://doi.org/10.1016/j.envpol.2011.02.046.

Houpert, L., P. Testor, X. Durrieu de Madron, et al. 2015. "Seasonal Cycle of the Mixed Layer, the Seasonal Thermocline and the Upper-Ocean Heat Storage Rate in the Mediterranean Sea Derived From Observations." *Progress in Oceanography* 132: 333–352. https://doi.org/10.1016/j.pocean.2014.11.004.

Hu, C., Z. Lee, and B. Franz. 2012. "Chlorophyll *a* Algorithms for Oligotrophic Oceans: A Novel Approach Based on Three-Band Reflectance Difference: A Novel Ocean Chlorophyll *a* Algorithm." *Journal of Geophysical Research* 117: 5545. https://doi.org/10.1029/2011JC007395

Huot, Y., and M. Babin. 2010. "Overview of Fluorescence Protocols: Theory, Basic Concepts, and Practice." In Chlorophyll a Fluorescence in Aquatic Sciences: Methods and Applications, 31–74. Netherlands: Springer.

Huot, Y., B. A. Franz, and M. Fradette. 2013. "Estimating Variability in the Quantum Yield of Sun-Induced Chlorophyll Fluorescence: A Global Analysis of Oceanic Waters." *Remote Sensing of Environment* 132: 238–253. https://doi.org/10.1016/j.rse.2013.01.003.

Kiefer, D. A., W. S. Chamberlin, and C. R. Booth. 1989. "Natural Fluorescence of Chlorophyll *a*: Relationship to Photosynthesis and Chlorophyll Concentration in the Western South Pacific Gyre." *Limnology and Oceanography* 34: 868–881. https://doi.org/10.4319/lo.1989.34.5.0868.

Kolber, Z., and P. G. Falkowski. 1993. "Use of Active Fluorescence to Estimate Phytoplankton Photosynthesis In Situ." *Limnology and Oceanography* 38: 1646–1665. https://doi.org/10.4319/lo.1993.38.8.1646.

Kromkamp, J. C., and R. M. Forster. 2003. "The Use of Variable Fluorescence Measurements in Aquatic Ecosystems: Differences between Multiple and Single Turnover Measuring Protocols and Suggested Terminology."

European Journal of Phycology 38: 103–112. https://doi.org/10.1080/0967026031000094094.

Laney, S. R., R. M. Letelier, and M. R. Abbott. 2005. "Parameterizing the Natural Fluorescence Kinetics of *Thalassiosira weissflogii*." *Limnology and Oceanography* 50: 1499–1510. https://doi.org/10.4319/lo.2005.50.5.1499.

Letelier, R. M., M. R. Abbott, and D. M. Karl. 1997. "Chlorophyll Fluorescence Response to Upwelling Events in the Southern Ocean." *Journal of Geophysical Research* 24: 409–412. https://doi.org/10.1029/97GL00205

Lin, H., F. I. Kuzminov, J. Park, S. Lee, P. G. Falkowski, and M. Y. Gorbunov. 2016. "Phytoplankton. The Fate of Photons Absorbed by Phytoplankton in the Global Ocean." *Science* 351: 264–267. https://doi.org/10.1126/science.aab2213.

Loftus, M. E., and H. H. Seliger. 1975. "Some Limitations of the In Vivo Fluorescence Technique." *Chesapeake Science* 16: 79. https://doi.org/10.2307/1350685.

Lutz, V., S. Sathyendaranath, E. Head, and W. K. W. Li. 2001. "Changes in the In Vivo Absorption and Fluorescence Excitation Spectra With Growth Irradiance in Three Species of Phytoplankton." *Journal of Plankton Research* 23: 555–569. https://doi.org/10.1093/plankt/23.6.555.

MacIntyre, H. L., T. M. Kana, T. Anning, and R. J. Geider. 2002. "Photoacclimation of Photosynthesis Irradiance Response Curves and Photosynthetic Pigments in Microalgae and Cyanobacteria." *Journal of Phycology* 38: 17–38. https://doi.org/10.1046/j.1529-8817.2002.00094.x.

Mezura-Montes, E., and C. A. Coello Coello. 2011. "Constraint-Handling in Nature-Inspired Numerical Optimization: Past, Present and Future." *Swarm and Evolutionary Computation* 1: 173–194. https://doi.org/10.1016/j.swevo.2011.10.001.

Morel, A. 1978. "Available, Usable, and Stored Radiant Energy in Relation to Marine Photosynthesis." *Deep Sea Research* 25: 673–688. https://doi.org/10.1016/0146-6291(78)90623-9.

Morel, A., and A. Bricaud. 1981. "Theoretical Results Concerning the Optics of Phytoplankton, With Special References to Remote Sensing Applications." In Oceanography From Space, edited by J. F. R. Gower, 313–327. NewYork: Plenum.

Morrison, J. R. 2003. "In Situ Determination of the Quantum Yield of Phytoplankton Chlorophyll *a* Fluorescence: A Simple Algorithm, Observations, and a Model." *Limnology and Oceanography* 48: 618–631. https://doi.org/10.4319/lo.2003.48.2.0618.

Morrison, J. R., and D. S. Goodwin. 2010. "Phytoplankton Photocompensation From Space-Based Fluorescence Measurements." *Geophysical Research Letters* 37: L06603. https://doi.org/10.1029/2009GL041799

Neville, R. A., and J. F. R. Gower. 1977. "Passive Remote Sensing of Phytoplankton Via Chlorophyll Fluorescence." *Journal of Geophysical Research* 82: 3487–3493. https://doi.org/10.1029/JC082i024p03487.

O'Malley, R. T., M. J. Behrenfeld, T. K. Westberry, A. J. Milligan, S. Shang, and J. Yan. 2014. "Geostationary Satellite Observations of Dynamic Phytoplankton Photophysiology." *Geophysica* 41: 5052-5059. https://doi.org/10.1002/2014GL060246.

Organelli, E., A. Bricaud, D. Antoine, and J. Uitz. 2013. "Multivariate Approach for the Retrieval of Phytoplankton Size Structure From Measured Light Absorption Spectra in the Mediterranean Sea (BOUSSOLE Site)." *Applied Optics* 52: 2257–2273. https://doi.org/10.1364/AO.52.002257.

Pedersen, M. E. H. 2010. Good Parameters for Particle Swarm Optimization Tech. Rep. HL1001, 1551–3203. Copenhagen, Denmark: Hvass Laboratories.

Platt, T., and S. Sathyendranath. 1993. "Estimators of Primary Production for Interpretation of Remotely Sensed Data on Ocean Color." *Journal of Geophysical Research* 98: 14561. https://doi.org/10.1029/93JC01001.

Roháček, K. 2002. "Chlorophyll Fluorescence Parameters: The Definitions, Photosynthetic Meaning, and Mutual Relationships." *Photosynthetica* 40: 13–29. https://doi.org/10.1023/A:1020125719386.

Ryther, J. H., and C. S. Yentsch. 1957. "The Estimation of Phytoplankton Production in the Ocean From Chlorophyll and Light Data." *Limnology and Oceanography* 2: 281–286. https://doi.org/10.1002/lno.1957.2.3.0281.

Ryu, J.-H., H.-J. Han, S. Cho, Y.-J. Park, and Y.-H. Ahn. 2012. "Overview of Geostationary Ocean Color Imager (GOCI) and GOCI Data Processing System (GDPS)." *Ocean Science Journal* 47: 223–233. https://doi.org/10.1007/s12601-012-0024-4.

Schallenberg, C., M. R. Lewis, D. E. Kelley, and J. J. Cullen. 2008. "Inferred Influence of Nutrient Availability on the Relationship Between Sun-Induced Chlorophyll Fluorescence and Incident Irradiance in the Bering Sea." *Journal of Geophysical Research* 113: C07046. https://doi.org/10.1029/2007JC004355

Schallenberg, C., R. F. Strzepek, N. Schuback, L. A. Clementson, P. W. Boyd, and T. W. Trull. 2020. "Diel Quenching of Southern Ocean Phytoplankton Fluorescence Is Related to Iron Limitation." *Biogeosciences* 17: 793–812. https://doi.org/10.5194/bg-17-793-2020.

Simis, S. G. H., Y. Huot, M. Babin, J. Seppälä, and L. Metsamaa. 2012. "Optimization of Variable Fluorescence Measurements of Phytoplankton Communities With Cyanobacteria." *Photosynthesis Research* 112: 13–30. https://doi.org/10.1007/s11120-012-9729-6.

Suggett, D. J., C. M. Moore, A. E. Hickman, and R. J. Geider. 2009. "Interpretation of Fast Repetition Rate (FRR) Fluorescence: Signatures of Phytoplankton Community Structure Versus Physiological State." *Marine Ecology Progress Series* 376: 1–19. https://doi.org/10.3354/meps07830.

Thuillier, G., M. Herse, P. Simon, et al. 1998. "The Visible Solar Spectral Irradiance From 350 to 850 nm as Measured by the SOLSPEC Spectrometer During the ATLAS I Mission." *Solar Physics* 177: 41–61. https://doi.org/10.1023/A:1004953215589.

Ugray, Z., L. Lasdon, J. Plummer, F. Glover, J. Kelly, and R. Martí. 2007. "Scatter Search and Local NLP Solvers: A Multistart Framework for Global Optimization." *INFORMS Journal on Computing* 19: 328–340. https://doi.org/10.1287/ijoc.1060.0175.

Wu, J., J. I. Goes, H. do Rosario Gomes, et al. 2022. "Estimates of Diurnal and Daily Net Primary Productivity Using the Geostationary Ocean Color Imager (GOCI) Data." *Remote Sensing of Environment* 280: 113183. https://doi.org/10.1016/j.rse.2022.113183.

Supporting Information

Additional Supporting Information may be found in the online version of this article.

Submitted 17 July 2024
Revised 16 October 2024
Accepted 27 January 2025